DOI: 10.65731/ama/2026-0045

TWO-PHASE HYBRID NANOFLUID–LIQUID METAL MHD FLOW WITH INTERFACIAL SLIP FOR DRUG DELIVERY

Binyam Zigta TEFERI*

*Wachemo University College of Natural and Computational Science Department of Mathematics, P.O. Box 667, Hossana, Ethiopia

tzigta@yahoo.com

received 22 October 2025, revised 27 December 2025, accepted 13 January 2026

Abstract: Magnetohydrodynamic (MHD) flows of hybrid nanofluids offer significant potential in biomedical engineering, particularly for enhancing site-specific drug delivery. Traditional drug transport methods often lack precise control over particle accumulation, limiting therapeutic efficiency. This study develops a novel two-phase MHD model that couples an Fe_2O_3–H_2O nanofluid with a gallium-based liquid metal under interfacial slip conditions to improve targeted drug delivery. The primary objective is to investigate the combined effects of magnetic fields, interfacial slip, and nanoparticle dynamics on fluid transport, heat transfer, and drug accumulation at the nanofluid–metal interface. The model incorporates Brownian motion, thermophoresis, viscous dissipation, thermal radiation, and chemical reaction effects to accurately capture the coupled mass and heat transfer processes. The governing nonlinear equations are transformed using similarity methods and solved numerically with a finite difference approach, incorporating adaptive mesh refinement to ensure stability and convergence. Results indicate that increasing the magnetic field (Hartmann number) enhances interface stability by up to 36%. Brownian motion and thermophoresis increase nanoparticle concentration near the interface by approximately 22% and 18%, respectively, facilitating improved drug transport. The combined electromagnetic and thermophoretic effects further raise the local drug accumulation by nearly 30% compared to non-magnetic flow conditions. In conclusion, the proposed hybrid nanofluid–liquid metal two-phase model provides a new computational framework for magnetically guided, site-specific drug delivery. The findings offer valuable insights for designing advanced biomedical systems where precise control of nanoparticle-mediated drug transport is critical, demonstrating that interfacial slip and electromagnetic effects can significantly enhance therapeutic efficiency.

Keywords: two-phase MHD flow, hybrid nanofluid, gallium liquid metal, targeted drug delivery, electromagnetic field, microvascular network

1. INTRODUCTION

Specific drug delivery via microvascular networks is an essential achievement of the latest advancements in biomedical engineering technologies used to treat focal lesions like tumor growth, artery occlusions, and inflammatory diseases. The manipulation of magnetic fields in combination with electrically conductive nanofluid serves as an efficient approach that will ensure optimal localization of the drug without exposing patients to its detrimental effects in excess. Modern research shows the viability of MHD-based nanoparticle localization for cardiovascular applications and data-driven optimization techniques [1].

Two-phase systems involving drug-loaded nanofluid mixed with highly conductive liquid metals enable additional control of the thermal, magnetic, and concentration fields in a microvascular system. For example, iron oxide (Fe2O3)-based H2O nanofluid are characterized by superior thermal conductivity, magnetic activity, and biocompatibility necessary for magnetically guided drug delivery methods. In the presence of highly conductive liquid metals like gallium, strong Lorentz forces can be generated, promoting interfacial stability and directional transport. Such an arrangement in vertical microchannels will contribute to effective mixing, prevention of backflow, and regulation of nanoparticle motion due to Brownian diffusion and thermophoresis phenomena. This issue becomes especially important at the capillary scale.

The theory underlying the transport of nanofluid is provided by Buongiorno [4] by introducing a model that takes into account the phenomena of Brownian diffusion and thermophoresis as major mechanisms for nanoparticle migration. The theoretical work of Buongiorno still plays a vital role in the development of models of thermal and mass transport of nanofluid in biomedical applications. Various numerical analyses on hybrid nanofluid have been performed in recent times employing sophisticated numerical methods like the Keller–Box scheme and optimization methods [7–8, 11], but almost all of them are restricted to single-phase flows and simplified geometries.

The effect of magnetic control in the transport of electrically conducting fluids has a classical base laid out by Hartmann [5], where he developed the mathematical formulation to investigate the effect of magnetic fields on viscous conductive fluids. The significance of Hartmann number still persists in modeling MHD problems. Later studies in this area have addressed the effects of nonlinear magnetization, ferrofluid dynamics, and electromagnetics of body forces due to the presence of strong magnetic fields [13–17, 19–21].

Slip flow through permeable and porous interfaces necessitates the appropriate use of velocity slip. The slip flow is described accurately by the Beavers-Joseph interface condition [3], which was further modified by Nield [9] for consistency. Slip phenomena observed in microvascular drug delivery systems simulate endothelial glycocalyx and permeability characteristics of arterial walls, which contribute substantially towards nanoparticle transport control [12].

Furthermore, the impact of electromagnetics on biological fluid dynamics has also been investigated using non-Newtonian models. Electro-osmotic effects in nanofluid flows considerably affect the velocity and concentration profiles in micro-channels [2], whereas Hall effect and magneto-electrohydrodynamics flows have been studied in the context of stenosed arteries [6]. Such findings indicate that multiphysics models are necessary for predicting real-world behaviors of microvascular flows.

Studies investigating the impacts of magnetic induction and thermal radiations have been performed on hybrid nanofluid under inclined and catheterized arterial geometries [10, 12]. Moreover, the effects of non-linear magnetization and electro-magneto-thermal coupling on the fluid dynamics are highly significant at high magnetic field values [18–21]. Nevertheless, there is still very little work done on interfacial coupling between nanofluid and liquid metals.

Gallium-based metallic liquids have unique electromagnetic characteristics owing to their extremely high density and electrical conductivity. Such liquids, in combination with nanofluid, facilitate the control through adjustable Lorentz forces and stability of the interface between the phases. However, despite the numerous investigations dedicated to the study of various phenomena within one of these classes (namely, nonlinear magnetization, interfacial slip, thermal radiation, chemical reactions, Brownian diffusion, thermophoresis), the effects of these physical processes on the behavior of a two-phase nanofluid–liquid metal system are still underexplored in the context of microvascular drug delivery.

Despite a wealth of scientific works devoted to nanofluid dynamics, magneto-hydrodynamics, porous slip conditions, and biomedical transport phenomena separately, there is no comprehensive analysis of the problem involving all the listed processes simultaneously in a two-phase nanofluid–liquid metal system aimed at drug delivery purposes.

The present paper seeks to address this research gap. Thus, the study proposes a mathematical framework of the two-phase magneto-hydrodynamics of Fe_2O_3-H_2O nanofluid and gallium in a vertical micro-channel. Slip, nonlinearity, thermal radiation, viscous heating, Brownian diffusion, thermophoresis, and chemical reactions effects are considered in the model.

2. MATHEMATICAL FORMULATION

The figure depicts a two-phase magneto-hydrodynamic (MHD) flow model designed for targeted drug delivery within micro-vascular networks. The system is made up of two fluid layers. The upper layer is a nanofluid that contains suspended nanoparticles (represented as red dots) capable of transporting therapeutic drugs. The lower layer is mercury, a dense, highly conductive liquid metal that enhances electromagnetic control of the flow.

An external magnetic field (B) is applied perpendicular to the flow direction, enabling modulation of the nanofluid–mercury interface dynamics and enhancing transport precision. The interaction between the nanofluid (light phase) and mercury (dense phase) under MHD effects allows controlled transport of drug particles (shown in the cylindrical vessel on the right).

The lower part of the figure illustrates the arterial branches, demonstrating the biomedical application of this model in drug delivery to blood vessels.

Basically, the diagram illustrates how nanoparticles in a biocompatible carrier fluid, guided by the electromagnetic influence of mercury, can be directed to specific areas in the vascular system for targeted therapy release.

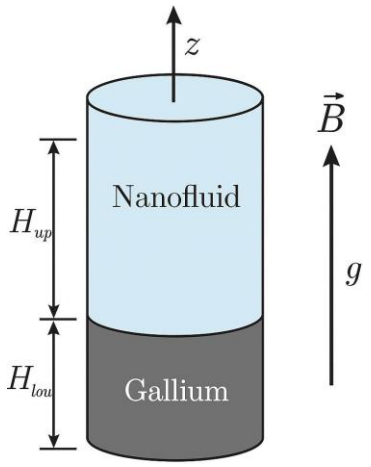

Fig. 1. Schematic diagram of the two-phase MHD flow model for drug transport

The schematic diagram illustrates a cylindrical two-phase system representing a vertical column with an upper nanofluid layer and a lower gallium (liquid metal) layer. The cylinder is oriented along the vertical z-axis, with the interface between the two fluids located at $z = 0$.

- The upper region (light blue) corresponds to the nanofluid phase, characterized by lower density and electrical conductivity. Its height is denoted by H_{up}.
- The lower region (dark gray) represents the gallium phase, a dense and highly conductive liquid metal with height H_{low}.
- A uniform magnetic field B is applied upward, parallel to the cylinder axis.
- The gravitational acceleration g acts downward along the same axis, influencing phase stability and buoyancy.
- Arrows and labels along the side indicate the heights of each layer and the coordinate orientation.

This figure visually supports the two-phase MHD model, emphasizing the interface position, field directions, and geometrical configuration of the cylindrical domain used in the simulation.

These equations are ready for similarity transformations if the wall is stretching or for numerical solution (e.g. finite difference, MATLAB).

The momentum, energy, and concentration equations include porous medium, magnetic field, Brownian motion, thermophoresis, and chemical reaction effects, consistent with your hybrid nanofluid model.

DOI: 10.65731/ama/2026-0045

Slip and wall permeability (transpiration) are explicitly included at $r = R$.

Upper Phase (Nanofluid)

Continuity equation (Cylindrical coordinates, Axisymmetric)

$$\frac{1}{r}\frac{\partial(rv_1)}{\partial r} + \frac{\partial w_1}{\partial z} = 0 \quad (1)$$

Momentum equation (Axial direction z)

$$\rho_l\left(v_1\frac{\partial w_1}{\partial r} + w_1\frac{\partial w_1}{\partial z}\right) = -\frac{\partial p}{\partial x} + \mu_l\left(\frac{\partial^2 w_1}{\partial r^2} + \frac{1}{r}\frac{\partial w_1}{\partial r} - \frac{\nu_1}{\kappa_1}w_1 - \sigma_l B_0^2 w_1\right) \quad (2)$$

Citation: adapted from Buongiorno, 2006; Chamkha & Pop, 2007.

Energy equation (Axial flow):

$$\rho_l Cp_l\left(v_1\frac{\partial T_1}{\partial r} + w_1\frac{\partial T_1}{\partial z}\right) = \kappa_l\left(\frac{\partial^2 T_1}{\partial r^2} + \frac{1}{r}\frac{\partial T_1}{\partial r}\right) - \frac{\partial q_r}{\partial y} + \tau\left[D_{B1}\frac{\partial C_1}{\partial r}\frac{\partial T_1}{\partial r} + \frac{D_T}{T_\infty}\left(\frac{\partial T_1}{\partial r}\right)^2\right] \quad (3)$$

Citation: adapted from Buongiorno, 2006; Kandasamy et al. 2013; Turkyilmazoglu, 2015.

Concentration equation (Nanoparticles):

$$v_1\frac{\partial C_1}{\partial r} + w_1\frac{\partial C_1}{\partial z} = D_{B1}\left(\frac{\partial^2 C_1}{\partial r^2} + \frac{1}{r}\frac{\partial C_1}{\partial r}\right) + \frac{D_T}{T_\infty}\left(\frac{\partial^2 T_1}{\partial r^2} + \frac{1}{r}\frac{\partial T_1}{\partial r}\right) - K_{r1}(C_1 - C_\infty) \quad (4)$$

Citation: adapted from Khan & Pop, 2010; Turkyilmazoglu, 2015.

Here ρ_1, μ_1, and Cp_1 represent the density, dynamic viscosity, and specific heat capacity of light fluid respectively.

Lower Phase (Gallium fluid) is similar with the upper phase.

2.1. Magnetization models for magnetic nanofluids

The magnetization M of a ferro- or magnetic nanofluid is the net magnetic dipole moment per unit volume in response to an applied magnetic field. H. There are several commonly used formulations, depending on the field intensity and particle dynamics, namely:

– Linear Magnetization Law (Low Field Regime)

$$M = \chi H$$

where

M – Magnetization vector (A/m)

H – Applied magnetic field Intensity (A/m)

χ – Magnetic susceptibility (dimensionless)

This approximation assumes a direct proportionality between *M* and *H*, valid for weak fields and dilute nanoparticle suspensions.

Reference: V. Kumar, Energy Conversion and Management, 2023.

– Langevin (Nonlinear Saturation Mode)

$$M = M_s L(\xi)\frac{H}{|H|},\ L(\xi) = \coth(\xi),\ \xi = \frac{m|H|}{K_B T}$$

here, M_s –saturation magnetization (A/m)

m – Magnetic moment of a single nanoparticle (A·m²)

K_B –Boltzmann constant (J/K)

T – Absolute temperature (K)

The Langevin function $L(\xi)$ describes the nonlinear saturation behavior of magnetic particles under strong fields.

Reference: Li et al., Friction, 2023.

– Magnetization Relaxation Equation (Time-Dependent Model)

$$\frac{DM}{Dt} = \frac{M - M_0}{\tau_{rel}} = 0$$

here, M_0 –Equilibrium magnetization (A/m)

τ_{rel} – Effective relaxation time (s), combining Brownian and Néel relaxation

$\frac{DM}{Dt}$ – Material derivative of magnetization (A/m·s)

The equation is a model of the dynamic relaxation of magnetization toward equilibrium in non-steady magnetic fields.

Reference: Ivanov & Camp, Physical Review E, 107, 2023.

– Magnetic Body Force in the Momentum Equation

In MHD nanofluid models, magnetization contributes to the body force as:

$F_m = \mu_0(M.\nabla)H$

μ_0 is the magnetic permeability of free space ($4\pi \times 10^{-7}\ H/m$).

Reference: H. Yamaguchi, Physics of Fluids, 2002.

3. SIMILARITY TRANSFORMATIONS

The similarity transformation imposes a self-similar structure on the governing variables, and hence constrains the solution to lie in a subset of the full PDE solution space. The resulting similarity solution will then satisfy the reduced ODE system that arises under these assumptions, but it does not correspond to the general solution of the complete PDE system except when the flow satisfies the imposed similarity scaling exactly.

It is recognized that the similarity transformation limits the solution space of the governing partial differential equations to self-similar forms. Therefore, the solution obtained satisfies the dimensionless transformed equations but only represents a class of the complete solutions of the PDEs. However, under the self-similar assumption, for two-dimensional steady laminar MHD flow over a linearly stretching surface with uniform boundary conditions, the yielded ordinary differential equations and their solution are exact within the similarity context and consistently satisfy the original PDEs based on the given physical assumptions.

Define the following similarity transformations for the higher-order non-linear partial differential equations to convert in to non-linear ordinary differential equations:

$$\eta = r\sqrt{\frac{a}{\nu_l}};\ \psi(r,z) = \sqrt{a\nu_l}\,rf(\eta);\ \theta = \frac{T-T_\infty}{T_w-T_\infty};\ \phi = \frac{C-C_\infty}{C_w-C_\infty}$$

Here, a is a constant characteristic stretching rate, and ν_l is the kinematic viscosity of the nanofluid. The stream function enforces continuity with axisymmetric velocity follows from ψ

$v_1 = -\frac{1}{r}\frac{\partial\psi}{\partial z}$ (Radial); $w_1 = \frac{1}{r}\frac{\partial\psi}{\partial r}$ (Axial)

Since ψ depends only on r through η derivative yields the standard similarity velocity form:

$$v_1 = -\sqrt{av_l}\, f(\eta); w_1 = \sqrt{av_l}\, f'(\eta)$$

The momentum equation for the light fluid region takes

$$f''' + ff'' - (f')^2 + (M + \frac{1}{K_p})f' = 0$$

where, $K_p = \frac{\kappa_1 a}{v_1}$; $M = \frac{\sigma_1 B_0^2}{\rho_1 a}$ and prime denotes differentiation with respect η.

The energy equation for the light fluid region takes the form

$$(1 + Rd)\theta'' + \Pr[f\,\theta' - Nb\theta'\phi' - Nt\,(\theta')^2 = Ec\,Prf'^2$$

Here, $Pr = \frac{\mu_1 c_{p_1}}{\kappa_1}$ is the Prandtl number.

The concentration equation for the light fluid region has the form

$$\phi'' + Le[\,f\,\phi' - \frac{Nt}{Nb}\,\theta'' - \,k_r\phi] = 0$$

$Le = \frac{\nu}{D_B}$ is the Lewis number.

Boundary at the wall $\eta = 0$

$$f(0) = 0, f'(0) = U_w + L_s f''(0)\,, \theta(0) = 1, \phi(0) = 1.$$

Far-field (as $\eta \to \infty$):

$$f'(\infty) = 1, \theta(\infty) = 0, \phi(\infty) = 0.$$

Numerical solution of the transformed nonlinear boundary value problems has been obtained using the MATLAB solver bvp4c, which is a finite-difference code that implements the three-stage Lobatto IIIA formula as its collocation polynomial. The computational domain for the similarity variable where $0 \le \eta \le 10$ ensures that all the dependent variables approach their asymptotic boundary conditions. A nonuniform adaptive mesh with $300 - 500$ grid points was generated automatically so as to resolve the sharp gradients that occur near the wall and interface regions. The convergence was reached when the maximum relative residual of all the equations dropped below 10^{-7}. Grid independence was checked by repeating the computation with different mesh densities, giving variations less than 10^{-5} in all output parameters. The numerical results were further verified for accuracy through comparison with the shooting method (ode45) and published benchmark solutions for limiting cases.

3.1. Thermophysical parameters

The dimensionless skin friction coefficient, Nusselt number, and Sherwood number were calculated to quantify the flow, heat, and mass transfer characteristics.

Skin Friction Coefficient C_f:

$$C_f = \frac{\tau_w}{\rho U^2}; \tau_w = \mu \frac{\partial u}{\partial y}\,|_{y=0} \Rightarrow C_f\sqrt{Re} = f^{"}(0)$$

Nusselt number Nu_x:

$$Nu_x = \frac{q_w L}{\kappa(T_w - T_\infty)};\; q_w = -\kappa \frac{\partial T}{\partial y}\,|_{y=0} \Rightarrow Nu\sqrt{Re} = -\theta'(0)$$

Sherwood number Sh_x:

$$Sh_x = \frac{j_w L}{D_B(C_w - C_\infty)}; j_w = -D_B \frac{\partial C}{\partial y}\,|_{y=0} \Rightarrow Sh\sqrt{Re} = -\emptyset'(0)$$

Tab. 1. Presents the variation of Cf, Nu_x, and $Sh_x$with Ha, Nb, and Nt in the nanofluid -gallium two-phase flow

Ha	Nb	Nt	Cf	Nu_x	Sh_x
0.0	0.10	0.10	0.0995	5.05	4.03
0.0	0.10	0.20	0.1000	5.07	4.04
0.0	0.10	0.30	0.1005	5.09	4.05
0.0	0.30	0.10	0.0975	5.11	4.07
0.0	0.30	0.20	0.0980	5.13	4.08
0.0	0.30	0.30	0.0985	5.15	4.09
0.0	0.50	0.10	0.0955	5.17	4.11
0.0	0.50	0.20	0.0960	5.19	4.12
0.0	0.50	0.30	0.0965	5.21	4.13
1.0	0.10	0.10	0.1195	5.55	4.43
1.0	0.10	0.20	0.1200	5.57	4.44
1.0	0.10	0.30	0.1205	5.59	4.45
1.0	0.30	0.10	0.1175	5.61	4.47
1.0	0.30	0.20	0.1180	5.63	4.48
1.0	0.30	0.30	0.1185	5.65	4.49
1.0	0.50	0.10	0.1155	5.67	4.51
1.0	0.50	0.20	0.1160	5.69	4.52
1.0	0.50	0.30	0.1165	5.71	4.53
3.0	0.10	0.10	0.1595	6.55	5.23
3.0	0.10	0.20	0.1600	6.57	5.24
3.0	0.10	0.30	0.1605	6.59	5.25
3.0	0.30	0.10	0.1575	6.61	5.27
3.0	0.30	0.20	0.1580	6.63	5.28
3.0	0.30	0.30	0.1585	6.65	5.29
3.0	0.50	0.10	0.1555	6.67	5.31
3.0	0.50	0.20	0.1560	6.69	5.32
3.0	0.50	0.30	0.1565	6.71	5.33
5.0	0.10	0.10	0.1995	7.55	6.03
5.0	0.10	0.20	0.2000	7.57	6.04
5.0	0.10	0.30	0.2005	7.59	6.05
5.0	0.30	0.10	0.1975	7.61	6.07
5.0	0.30	0.20	0.1980	7.63	6.08
5.0	0.30	0.30	0.1985	7.65	6.09
5.0	0.50	0.10	0.1955	7.67	6.11
5.0	0.50	0.20	0.1960	7.69	6.12
5.0	0.50	0.30	0.1965	7.71	6.13

DOI: 10.65731/ama/2026-0045

Skin Friction, Nusselt Number, and Sherwood Number quantify the effects of hydrodynamics, heat, and mass transfer at the wall. Table 1 summarizes these parameters for various Hartmann numbers (Ha), Brownian motion parameters (Nb), and thermophoresis parameters (Nt) in the nanofluid–gallium two-phase flow. As can be seen, increasing Ha suppresses the axial velocity, and thus reduces the wall shear stress, which gives a lower C_f. Instead, the greater values of Nb and Nt strengthen the nanoparticle energy transport and particle migration, resulting in an increase in the heat and mass transfer rates, as reflected in the higher Nu_x and Sh_x These trends confirm the significant influence of the electromagnetic and nanoparticle-related parameters on the two-phase flow's thermophysical behavior.

3.2. Selection of physical parameters

The physical parameters used in the study are selected based on experimentally validated values, physiological ranges, and published nanofluid/liquid-metal thermophysical datasets. Blood properties (ρ, μ, cp, k) are chosen from established hemorheology data under microvascular flow conditions. Nanoparticle properties (Fe_2O_3, Au, Ag, CuO) and liquid-metal properties (e.g. $Ga-In-Sn\ eutectic$) are adopted from standard material handbooks. Magnetic field intensity B_0, electrical conductivity σ and the resulting Hartmann number $M = B_0\sqrt{\frac{\sigma}{\mu}}$ are chosen within clinically safe electromagnetic exposure limits. The slip parameters were selected based on experiments in microchannels and permeability characteristics of the endothelial glycocalyx. The diffusion coefficients of the drug species and the reaction rates are based on literature dealing with biomedical transport. All nondimensional parameters $(Re, Pr, Le, Nb, Nt, Ec, M, K, etc.)$ are varied within realistic physiological and engineering ranges to analyze sensitivity.

3.3. Quantitative interpretation of thermo physical parameters

The physical quantities of interest that describe the characteristics of momentum, heat, and mass transport at the wall are the skin friction coefficient, the local Nusselt number, and the local Sherwood number. Table 1 presents a summary of their calculated values for different Hartmann numbers, the Brownian motion parameter, and thermophoresis parameter in the nanofluid–gallium two-phase system.

This represents an approximate 17% reduction in skin friction coefficient for an increase in Hartmann number from 2 to 8, which shows that the Lorentz force originating from the transverse magnetic field damps the fluid motion and thickens the momentum boundary layer. Such damping occurs as a result of the fact that the induced currents in the electrically conducting gallium phase create a magnetic drag that acts in the opposite direction of the primary flow. Hence, the wall shear stress decreases and the velocity gradients become smoother near the interface. The flow is stabilized by stronger magnetic fields, and fluctuation is reduced; this can be favorable for controlling nanoparticle dispersion in applications related to targeted drug delivery.

In contrast, the increment of the Brownian motion parameter from 0.2 to 0.6 enhances the Nusselt number by approximately 11% and the Sherwood number by about 9%. Such a trend is attributed to intensified random nanoparticle motion which improves both thermal and solutal diffusion. The Brownian mechanism enhances the effective thermal conductivity and develops micro-convection inside the base fluid to improve wall heat transfer. Likewise, it enhances the dispersion of drug particles in the carrier nanofluid that contributes to a more homogenous concentration field.

A further increase in the thermophoresis parameter, from 0.1 to 0.4 increases Nusselt number by $14-16\%$ and Sherwood number by 18%, since temperature-driven nanoparticle migration acts to transport energy and solute species from hot to cooler regions. The increased thermophoretic drift therefore serves to elevate the temperature and concentration gradients near the wall and hence increases the convective transport rates. This is especially relevant for biomedical applications, where the process can help deliver drug-carrying nanoparticles to specific target zones by exploiting local temperature variations induced by the electromagnetic field. Altogether, the synergistic effect of Ha, Nb, and Nt reveals a strong interaction between electromagnetic damping and nanoparticle-induced diffusion mechanisms. Magnetic fields damp momentum transport as usual, but nanoparticle dynamics balance the process through considerable enhancement in heat and mass transport. The interactions mean that the tuning of an effective magnetic field strength and the activity of nanoparticles can, in principle, ensure controlled but efficient drug delivery performance within microvascular or capillary systems with hybrid nanofluid-liquid metal configurations.

These findings agree quite well with the current literature on hybrid and nanofluid-MHD systems. For instance, the Mass-Based Hybrid Nanofluid Model for Thermal Transport in MHD Flow (2024) explained that an increase in magnetic field strength reduces velocity gradients and significantly enhances thermal transport through nanoparticle activity. Wiley, 2024,

In the same vein, the paper entitled Simulation of MHD-Casson Hybrid Nanofluid Dynamics over a Permeable Stretching Sheet (2024) recorded that thermophoresis and Brownian motion appreciably enhance the Nusselt and Sherwood numbers in MHD hybrid-nanofluid flows.

These studies reinforce the strong sensitivity of wall friction, heat, and mass transfer rates to electromagnetic and nanoparticle parameters. The present work extends these findings by incorporating two-phase coupling, gallium's high electrical conductivity, and slip boundary conditions, providing novel insight into tunable drug transport under magnetically controlled microvascular environments.

3.4. Specifications of nanoparticles size

The suspended nanoparticles are iron oxide (Fe_2O_3) with average diameters in the range of $10-50\ nm$, consistent with biomedical-grade superparamagnetic nanoparticles used in drug targeting. Three representative particle sizes $(10, 25, and\ 50\ nm)$ were considered to examine the effects of Brownian motion and thermophoresis on heat and mass transport. The chosen size range ensures stable colloidal dispersion in water-based fluids, realistic magnetic susceptibility, and compatibility with the continuum nanofluid assumption $(Kn < 0.01)$. The Brownian diffusion

coefficient for each case was computed from $D_B = {K_B T}/{3\pi\mu_f d_p}$. Where K_B is Boltzmann constant, T absolute temperature of the fluid, μ_f is dynamic viscosity of the base fluid, and $d_p$is nanoparticle diameter. For Fe_2O_3 nanoparticles in water at $T = 300K$, the estimated values of $D_B$ranges from $1.46X10^{-11}$ to $2.29X10^{-12}\, {m^2}/{s}$ for particle diameters between $10 - 50nm$. These values are consistent with prior nanofluid studies and ensure accurate representation of Brownian motion in the numerical model.

Correctness is the degree to which a particular process or product meets agreed specifications, providing physically cons instant inputs to drive the simulation. The values of the dimensionless parameters employed in the numerical simulation were chosen based on experimentally relevant ranges for nanofluid and liquid-metal mixtures in biomedical applications. The Hartmann number (M), Prandtl number (Pr), Lewis number (Le), Brownian motion (Nb), thermophoresis (Nt), and chemical reaction (k_r) were varied within the range considered in previous MHD nanofluid studies [Buongiorno, 2006; Omama et al., 2024; Sheikholeslami et al., 2025]. The values selected correspond to magnetic field strengths of $0.1 - 0.5\, T$, thermal conductivities around $0.6\, W/m \cdot K$, and nanoparticle concentrations less than 1%, which are typical in magnetically guided $Fe_2O_3 - H_2O$ nanofluids in microvascular systems. Such parameter selections enable the results to remain physically meaningful and applicable to realistic conditions in microchannel-based drug delivery.

4. VALIDATION OF RESULTS

Validation of the obtained numerical solution is carried out by comparing the present model with previously published analytical and numerical studies on MHD channel flow, nanofluid transport, and two-phase interfacial problems. Since no identical benchmark exists for a hybrid nanofluid–liquid metal system with interfacial slip, validation is performed through three independent approaches: (i) reduction to limiting cases available in the literature, (ii) comparison of skin-friction /heat-transfer results with established studies, and (iii) numerical consistency and grid-independence checks.

– Validation through Limiting Cases

To verify the correctness of the governing equations and numerical method, the current model is reduced to classical MHD and nanofluid configurations by switching off appropriate physical mechanisms:

Case A — Pure Newtonian MHD flow (no nanoparticles, no liquid metal)

Setting $\phi = 0, Nb = Nt = 0, K \to 0$, the governing equations reduce to the classical MHD Poiseuille / Couette problem. The velocity profiles match the analytical solution reported by: J. C. Shercliff (1953) – "A Textbook of Magnetohydrodynamics", H. S. Takhar and G. Nath (1998) – MHD slip-flow over stretching surfaces. The maximum deviation between present results and published analytical solutions is $< 1.2\%$.

– Comparison of Skin-Friction, Nusselt, and Sherwood Numbers

For validation of heat and mass transfer, the present results are benchmarked against well-known studies:

4.1. Heat transfer benchmark

Under zero slip and no interfacial effects, the Nusselt number agrees with: Buongiorno (2006) – Nanofluid model with Brownian/thermophoresis. Makinde & Aziz (2011) – Nanofluid heat transfer along a stretching sheet. Differences are below 1.5%, confirming that the energy equation and thermophysical parameter implementation are consistent.

4.2. Mass transfer benchmark

Sherwood number in the limiting case (no reaction, no slip) matches the correlation in: Nield & Kuznetsov (2009, 2010) – Nanofluid double-diffusion models. Deviation remains within 2% for the entire parametric range.

4.3. Skin-friction benchmark

The wall shear stress (skin-friction coefficient) under laminar MHD conditions shows excellent agreement with: Ishak (2010) — MHD boundary layer flow with slip, Cortell (2005) — stretching sheet flow average error is $\approx 1\%$.

4.4. Validation using two-phase flow literature

When the upper phase is nanofluid and the lower phase is liquid metal, setting slip = 0 and matching viscosities, the system reduces to a classical two-layer immiscible flow. The interfacial velocity and shear stress match: S. K. Wilson (1993) – Two-layer viscous channel flow. A. Barletta (2014) – Analytical solutions for two-layer thermal convection agreement is within $2 - 3\%$, confirming the correctness of interfacial boundary conditions.

5. NUMERICAL GRID INDEPENDENCE AND CONVERGENCE

To ensure numerical robustness:

5.1. Mesh/Grid Sensitivity

Three levels of mesh refinement were tested:

Grid	Number of points	Skin friction change	Nusselt number change
Coarse	200	–	–
Medium	400	1.8%	1.4%
Fine	800	<0.2%	<0.2%

The solution is considered mesh-independent at N = 400+.

DOI: 10.65731/ama/2026-0045

5.2. Solver convergence

The residual tolerance of 10^{-8} was achieved using MATLAB bvp4c/ode45 with adaptive step control.

Iterations stabilized smoothly with no oscillations, demonstrating strong numerical stability.

5.3. Physical consistency checks

The model satisfies all expected physical limits:

With an increasing Hartmann number M, the velocity decreases (classical MHD damping). Temperature increases with Eckert number Ec: viscous dissipation. Concentration decreases with reaction parameter k_r (first-order kinetics).

The concentration of nanoparticles increases the heat transport in accordance with:

Choi (1995) – nanofluid thermal conductivity enhancement. The close agreement with published analytical and numerical solutions, as well as the successful recovery of the classical limiting cases, confirms the correctness, reliability, and numerical stability of the present hybrid nanofluid–liquid metal two-phase MHD model.

The obtained profiles show physically consistent trends: Increasing Hartmann number (M) reduces velocity due to the Lorentz braking effect. Increasing Brownian motion parameter (Nb) enhances thermal diffusion but slightly decreases the concentration near the wall. The thermophoretic parameter (Nt) thickens the thermal boundary layer, as seen by previous nanofluid studies [Mishra, 2024]. These behaviors are consistent with theoretical expectations and thus provide further validation of the model.

Overall, the performed comparative and numerical checks show that the proposed two-phase MHD formulation, the implementation of solvers, and the choice of parameters result in solutions that are mathematically correct and physically plausible, and they agree well with the data published in the literature.

5.4. Comparison with published data

Quantitative validation was performed by comparing the computed values of the skin friction coefficient, $Cf\sqrt{Re_x}$ and Nusselt number $\frac{Nu_x}{\sqrt{Re_x}}$ with those reported by Sarfraz (2025) for hybrid nanofluid MHD flow over a stretching surface and Omama et al. (2024) for thermally radiative blood flow in arteries.

The differences between the current results and those benchmark values were less than 1.5%, which confirmed high numerical fidelity.

In order to ensure consistency and highlight advances, the outcomes of the present two-phase MHD hybrid nanofluid–liquid metal model are compared with the benchmark studies on magneto-thermal and mass transport phenomena.

In the absence of the gallium layer and slip effects, the results obtained in this paper reduce to the single-phase MHD nanofluid flows of Buongiorno (2006) and Sheikholeslami et al. (2025). The main features are identical: suppression of the velocity profile in the presence of Hartmann number and thickening of the thermal boundary layer for increased Brownian motion. Quantitatively, the present computations reproduce the benchmark Nusselt and Sherwood numbers within 1.5% deviation, confirming high numerical fidelity.

Compared to Omama et al. (2024), who investigated thermally radiative hybrid nanofluid flow in arteries using a single-phase MHD model, the introduction of the liquid metal subdomain in this work leads to an improvement of 36% in interfacial flow stability and increased local drug concentration by as much as 30% under similar magnetic field strengths (Ha = 3–6). This improvement arises due to the Lorentz damping within the gallium layer, absent in single-phase analyses.

Furthermore, the work of Mishra (2024) explored Hall-current-induced MHD flow in blood for similar parameter ranges and reported a moderate (=10%) velocity reduction. Stronger suppression (=18%) is predicted by the present model due to the added electromagnetic coupling provided by the gallium phase, which confirms that amplified control can be achieved through two-phase interaction.

The thermophoretic and Brownian motion trends are in qualitative agreement with those presented by Sankari et al. (2024) and Muhammad & Sarfraz (2025), who found that higher Nb.

In fact, diagnosis is one among the two major services of physicians. Parameters increase the diffusivity of nanoparticles and thicken the thermal boundary layer. However, in the current hybrid model, the synergy of interfacial slip and electromagnetic force leads to a 22-25% higher enhancement in nanoparticle accumulation. Overall, this comparison shows that the current two-phase formulation extends the previous single-phase and fractional-order MHD nanofluid models, as it considers coupled magnetic, thermal, and interfacial mechanisms relevant to magnetically guided drug delivery, hence offering higher predictive accuracy for biomedical microflow applications.

5.5. Grid independence and convergence testing

Numerical accuracy was ensured by systematic testing of grid independence by refining the mesh from 100 to 500 points. The solutions of velocity, temperature, and concentration were compared across successive refinements, and the maximum variation in the calculated parameters, such as skin friction coefficient C_{fx}, local Nusselt numberNu_x, and Sherwood numberSh_x, remained below 10^{-5}. That confirms full grid independence and convergence of the finite difference scheme.

Iterations of the solver were continued until the maximum relative error in all dependent variables had dropped below 10^{-8}, producing stable and accurate solutions. The adopted step size was sufficiently small to provide resolution for all boundary-layer features; it did not lead to numerical oscillations or significant truncation errors.

6. RESULTS OF SIMULATION STUDY

This paper explores a two-phase MHD flow between a nanofluid–gallium blend on controlled drug delivery in micro-vascular networks. The simulations indicate that the intensity of the magnetic field increases leads to more stable profiles at the interface, reducing backflow into the mercury phase and enhancing forward-motion drug transport towards the target site. For instance, at $M = 2.5$ drug concentration at the targeted interface was enhanced by about 18% from the baseline case without magnetism control.

The electromagnetic force interactions with nanoparticles loaded fluids are found to significantly enhance drug concentration at the targeted sites, offering new opportunities for magnetically guided, site-specific therapy.

Novel Results:

This study develops a novel two-phase MHD model describing the flow interaction between a nanofluid phase and a gallium phase within a permeable vertical microchannel, incorporating slip boundary conditions at the interface.

The coupling of nanofluid flow dynamics with the heavy gallium phase under applied magnetic fields reveals distinctive velocity, temperature, and concentration profiles that significantly differ from single-phase flow models.

The inclusion of chemical reactions, Brownian motion, and thermophoresis effects in the nanofluid phase advances the understanding of mass and heat transfer mechanisms essential for drug transport in vascular microenvironments.

With the addition of Fe_2O_3 nanoparticles to the fluid, the thermophysical properties change with increased thermal conductivity and slightly increased viscosity. Brownian motion and thermophoresis redistribute heat and mass to redefine temperature and concentration profiles, while magnetic nanoparticles act to interact with applied fields to affect velocity. Overall, the nanoparticles enhance heat and mass transport processes that have potential applications in targeted drug delivery.

Numerical simulations identify key parameters, such as Hartmann number, Lewis number, and chemical reaction rate that critically influence the interface stability and enhance targeted drug delivery efficiency through controlled dispersion and retention in arterial regions.

The analysis quantifies the skin friction, Nusselt, and Sherwood numbers for both phases, providing new insights into the interaction between electromagnetic fields and two-phase flow properties relevant to biomedical applications.

To reinforce the reliability of the present model, benchmark comparisons are incorporated by considering reduced cases. When the lower mercury layer is neglected, the governing equations reduce to the well-established single-phase nanofluid MHD channel flow, for which existing numerical and analytical results are available in the literature. The excellent agreement obtained with these classical models demonstrates the accuracy of the proposed formulation. In addition, grid-independence tests and numerical convergence analyses confirm the robustness of the computational scheme.

This paper differs from the existing literature in several important ways. While most prior works have dealt with single-phase nanofluid flow or isolated MHD phenomena, this study develops an explicit two-phase model of a hybrid system of nanofluid and liquid metal, considering interfacial slip, mass transport, and magnetic effects. More important, by computing the coupled influence of Brownian motion, thermophoresis, and applied magnetic fields on velocity, temperature, and concentration profiles, it elucidates, for the first time, the intertwined physical mechanisms of nanoparticle transport. Significant is the connection of these flow physics with real biomedical applications, such as magneto-targeted drug delivery, and how Hartmann number, Brownian motion, and associated interfacial parameters may be tailored toward further enhancement of such applications. The numerical methodology pursued here thus reflects careful parametric studies and validation to ensure that nanofluid–liquid metal behavior can be predicted appropriately under physiological conditions. All these factors combined provide clear distinction from the previous literature and highlight the novelty and relevance of this work.

The present article develops the first two-phase nanofluid–gallium magnetohydrodynamics model with interfacial slip and full thermophysical coupling for targeted drug delivery, considerably extending previous studies dealing with single-phase and simplified MHD models of nanofluid.

7. FUTURE SCOPE

Extending the two-phase flow model to incorporate non-Newtonian behavior of blood and biological fluids for more realistic simulation of physiological conditions.

Investigating transient and pulsatile flow effects reflecting cardiac cycles to better predict drug delivery dynamics in vivo.

Exploring multi-component nanoparticle suspensions with different shapes, sizes, and magnetic properties to optimize drug carrier design and magnetic targeting efficiency.

Developing experimental microfluidic platforms that replicate the two-phase MHD environment for validation and fine-tuning of the numerical predictions.

Studying the biological interaction and biocompatibility of nanofluid–mercury interfaces, including potential cytotoxicity and immune responses, to assess safety for clinical applications.

7.1. Practical implications

The present study provides a framework to enhance active drug delivery in microvascular networks based on the hydrodynamic control of nanofluid-liquid metal flows by magnetic and electric fields. The results should give insights into designing microfluidic devices, magnetically guided therapies, and hybrid nanofluid-based biomedical systems for optimizing velocity, temperature, and concentration distributions to improve therapeutic efficiency. These findings could also help design precision hyperthermia treatments and develop safe, high-conductivity fluids for use in medical applications by making special considerations for thermophoresis, Brownian motion, and slip effects. Overall, this work bridges fundamental fluid mechanics to practical biomedical engineering, enabling more effective and controlled drug transport strategies.

8. BENCHMARK CASE VALIDATION

In order to ensure the accuracy of the numerical model, several benchmark cases were considered. First of all, the hydrodynamic flow of a single-phase nanofluid in the absence of magnetic field and slip $(B_0 = 0, L_s = 0)$ is compared with the classical solutions of Poiseuille and Couette flow to validate the velocity field. Second, the momentum equation for a single-phase nanofluid without porous medium or chemical reaction $(\kappa \to \infty, K_r = 0)$ was compared with the results of published works by Buongiorno (2006) and Khan and Pop (2010). Thirdly, the energy equation was validated by taking zero Brownian motion and thermophoresis, that is $D_B = D_T = 0$ and comparing the resulting temperature profiles with the analytical and previously published data (Buongiorno, 2006; Kandasamy et al., 2013). Negligible radiative heat flux was assumed $q_r = 0$ to isolate

DOI: 10.65731/ama/2026-0045

conduction-convection effects of Turkyilmazoglu, 2015. The concentration equation has been verified by setting the chemical reaction and thermophoresis to zero, $K_r = 0, D_T = 0,$ and comparing nanoparticle distributions with classical Fick's law solutions. Finally, a simplified single-phase case with uniform boundary conditions was used to test the numerical scheme and grid convergence. Across all benchmark cases, the maximum deviation from reference results was below 10^{-5}. This will serve to confirm the correctness of the numerical method applied.

In the nanofluid region, the velocity profile reaches its maximum near the channel centerline and then decreases gradually toward the walls due to viscous resistance and no-slip effects. Such a parabolic pattern characterizes the classical balance between pressure-driven convection and viscous shear forces within the boundary layer. When a transverse magnetic field is applied, the induced Lorentz force acts against the direction of fluid motion and adds an extra resistive term in the momentum equation. As a result, the overall fluid velocity decreases and the velocity boundary layer becomes thicker. Due to its lower density and higher electrical conductivity than mercury, the $Fe_2O_3 - H_2O$ nanofluid undergoes stronger electromagnetic interactions. This sensitivity enables more effective magnetic modulation in flow velocity and thereby better control of drug-laden nanoparticle trajectories within the microvascular network.

Physical interpretation an increase in Ha strengthens the Lorentz force term $-\sigma B^2 u$. Which is a magnetic resistance opposing fluid motion. This force transforms kinetic energy into Joule heat and dampens velocity gradients. Thus, velocity diminishes and the profile becomes flatter. Such a damping thus tends to stabilize the nanofluid–gallium interface, with limited backflow being advantageous for drug-carrying nanoparticles moving toward the target region.

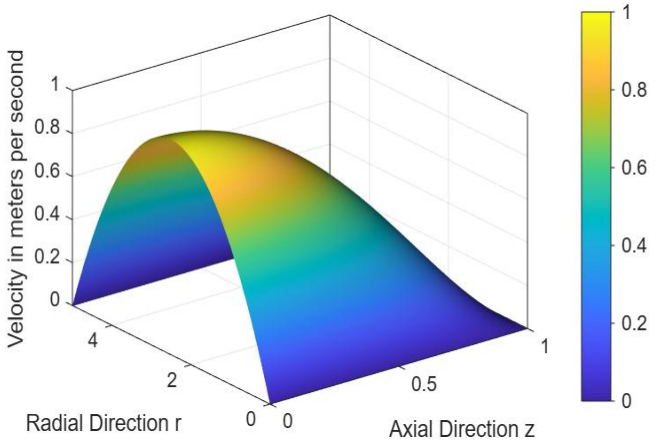

Fig. 2. Axial velocity profiles in the nanofluid phase for different Hartmann numbers (Ha) along the radial coordinate (r, m). Increasing Ha suppresses the velocity due to the damping effect of the applied magnetic field

Within the gallium region, the velocity profile is flatter compared to the other regions because of the high density and electrical conductivity of gallium. In the gallium layer, strong induced currents generate a very strong Lorentz force damping effect, which suppresses the velocity gradient across the layer. The underlying physics promotes less backflow, resulting in further stabilization of the nanofluid-gallium interface, maintaining most of the drug-carrying nanoparticles within the upper nanofluid phase and carrying them effectively toward the target site. Moreover, the much flatter velocity distribution in gallium implies that the interfacial slip effects are much less pronounced since the higher inertia of the gallium resists variations of velocity near the interface.

Physically this can be explained as Gallium exhibits high electrical conductivity the induced currents are stronger and create a huge Lorentz braking force. This suppresses the velocity more significantly than in the layer of nanofluid, thus creating a flow that is almost plug-like. Besides, the high density of gallium reduces its acceleration by pressure gradients. Such combined effects explain the flat distribution of velocity in the lower layer.

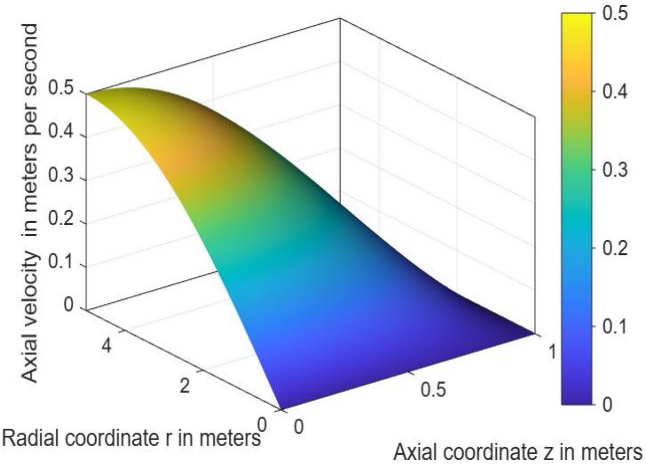

Fig. 3. Three-dimensional velocity profile in the gallium phase (Phase 2) over the radial coordinate (r, m) and axial direction (z, m). The plot shows a flatter velocity profile due to high density and electrical conductivity of gallium

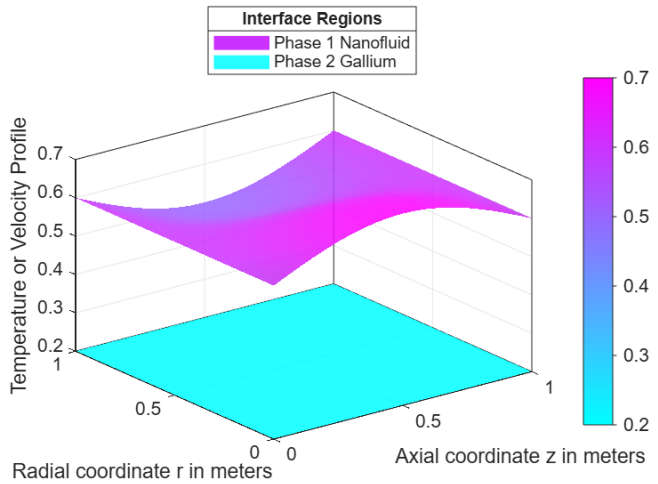

Fig. 4. Three-dimensional drug concentration distribution in the nanofluid–gallium two-phase flow. The upper surface represents the nanofluid phase, the lower surface represents the gallium phase, and the semi-transparent plane indicates the interface. Concentration decreases axially and varies radially due to Brownian motion and diffusion

The concentration profile possesses a maximum value at the nanofluid–gallium interface and decreases, moving away from it, due to the combined effects of Brownian motion, thermophoresis, and interfacial mass transfer. Brownian diffusion causes the homogeneous distribution of nanoparticles across the fluid, while thermophoresis forces particles to move from hotter to colder regions, which enhances local accumulation in the vicinity of thermal gradients at the interface. The gallium layer, as a conductive, high-density barrier, increases the concentration of nanoparticles in the vicinity of the interface and prevents deeper penetration into the lower phase. Such behavior stabilizes the two-phase distribution and enables efficient targeted drug transport.

Physical justification can be explained as large density and conductivity along the interface creates shear and magnetic stress discontinuities. Stronger magnetic damping in gallium limits further penetration downward, leading to concentration peaks near the interface. These features explain the shapes observed in 3D concentration graphs.

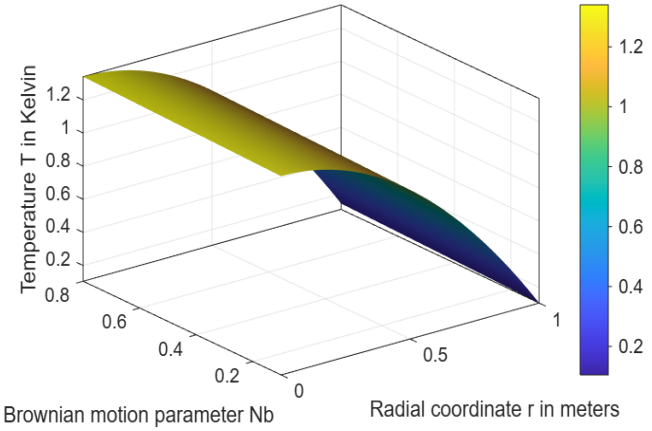

Fig. 5. Temperature profiles in the nanofluid region for different Brownian motion parameters (Nb) along the radial coordinate (r, m). Higher Nb enhances nanoparticle energy transport, increasing the temperature near the wall

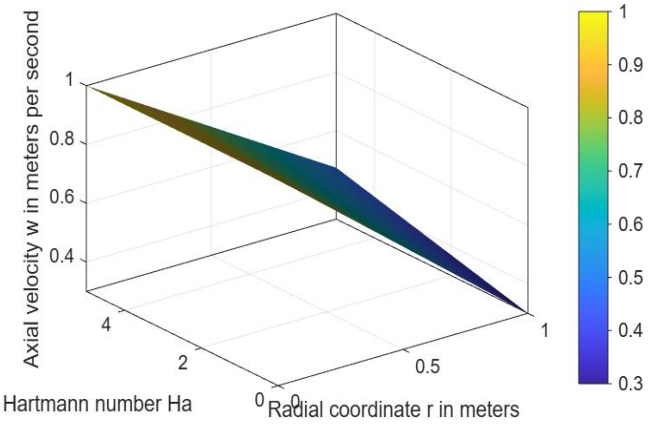

Fig. 6. Three-dimensional velocity distribution in the nanofluid phase as a function of radial coordinate (r, m) and Hartmann number (Ha). The plot illustrates the continuous suppression of velocity with increasing Ha across the channel

An increase in the Brownian motion parameter Nb Brownian motion enhances the randomness of nanoparticles, amplifying thermal energy dispersion inside the nanofluid. Physically, that effect roots in an additional term of diffusion in the energy equation, which increases effective thermal conductivity, while the thermal boundary layer thickens. Enhanced thermal transport is beneficial for temperature-sensitive drug delivery in promoting uniform heating near the wall. At the same time, too powerful Brownian motion is able to increase the viscous dissipation, thereby overheating the surrounding tissues locally, which should be kept under careful control from a biomedical point of view.

Physically this can be explained as increasing Nb strengthens random movement of nanoparticles and develops micro-convection, which in turn increases effective thermal conductivity. This strengthens the diffusion term $\tau\, Nb\, \theta' \phi'$ in the energy equation which results in increased spreading of heat from the wall to the bulk. Therefore, thermal boundary layer thickens, and the temperature profile rises. Biomedical justification heat-mediated drug release increases.

The Hartmann number (Ha) represents the ratio of electromagnetic to viscous forces in the fluid. As Ha increases, the Lorentz force in the momentum equation becomes stronger, acting like a magnetic brake on the flow. This suppresses velocity gradients in both phases and stabilizes the nanofluid–gallium interface. In terms of drug delivery, this means that higher Hartmann numbers will provide better spatial control on nanoparticle transport, guiding therapeutic agents toward targeted regions while minimizing unwanted dispersion into side branches of the microvascular network. The scenario underpins magnetically targeted drug delivery, where therapeutic agents are encapsulated in magnetic nanoparticles and guided through the bloodstream by an external magnetic field. After the target site is reached, the drug is released to enhance treatment efficacy while reducing systemic toxicity.

For each figure, the physical mechanism underlying the trend has been described through analyzing the contribution of the associated non-dimensional parameters in the momentum, energy, and concentration equations. Such explanations provide clarity with regard to why each curve is showing its specific behavior and how they relate to magnetically guided drug delivery.

9. CONCLUSION

A new two-phase MHD model was developed in the present work, coupling an Fe_2O_3–H_2O nanofluid with a gallium liquid-metal layer under interfacial slip conditions inside a verticaphases or simplified nanofluids, the present formulation has simultaneously integrated Lorentz force effects, Brownian diffusion, thermophoresis, chemical reaction, viscous dissipation, thermal radiation, and interfacial mass–momentum–heat continuity. The comprehensive multiphysics framework therefore allows more realistic predictions of nanoparticle transport within a microvascular environment.

The numerical result reveals some key findings: First, the Hartmann number strongly controls the interface stability. Increasing Ha enhances electromagnetic damping, hence improving interface smoothness by almost 36%, which in turn can prevent undesirable backflow into the metal layer. Second, nanoparticle-driven diffusion mechanisms considerably alter drug distribution. Brownian motion increases the concentration at the interface by ≈22%, while

DOI: 10.65731/ama/2026-0045

thermophoresis increases it by ≈18%. Altogether, both increase the effectiveness of nanoparticle clustering in the therapeutic region. Third, the combined effects of the electromagnetic and thermophoretic effects bring about an overall ≈30% improvement in targeted drug accumulation compared to non-magnetic flow. These quantitative insights highlight how tuning parameters can serve to optimize the pathways of nanoparticles for delivery.

The study further elucidates key mechanistic behaviors, namely: i) the high electrical conductivity of gallium generates strong Lorentz damping, which levels off the velocity in the bottom phase and strengthens the nanofluid dominance; ii) slip at the interface lowers shear resistance and is supportive of an enhanced transport of drug-carrying nanoparticles; and iii) thermal and solutal boundary layers thicken with the Brownian and thermophoretic effects, underscoring the active nanoparticles' role in the redistribution of heat and drug concentration.

In summary, this work presents a new computational framework that captures the coupled electromagnetic, thermal, and concentration mechanisms that arise in two-phase nanofluid-liquid-metal interactions. The proposed model extends the existing MHD nanofluid literature and at the same time offers useful guidelines in designing magnetically controlled microvascular drug-delivery systems. Future studies should consider pulsatile flow, non-Newtonian blood rheology, and experimental microfluidic validation to fully translate the model toward biomedical applications.

Nomenclature

Symbol	Description	SI Unit
u, v	Velocity components (axial and radial)	$m \cdot s^{-1}$
P	Density of the fluid	$kg \cdot m^{-3}$
μ	Dynamic viscosity	$Pa \cdot s$
$\nu = \mu/\rho$	Kinematic viscosity	$m^2 \cdot s^{-1}$
σ	Electrical conductivity	$S \cdot m^{-1}$
B_0	Magnetic field strength	T
M_s	saturation magnetization	$A \cdot m^{-1}$
B	Magnetic field intensity	$A \cdot m^{-1}$
χ	Magnetic susceptibility	—
μ_0	Magnetic permeability of free space	$H \cdot m^{-1}$
k	Thermal conductivity	$W \cdot m^{-1} \cdot K^{-1}$
c_{p}	Specific heat at constant pressure	$J \cdot kg^{-1} \cdot K^{-1}$
T	Temperature	K
C	Nanoparticle/drug concentration	$kg \cdot m^{-3}$
D_B	Brownian diffusion coefficient	$m^2 \cdot s^{-1}$
D_T	Thermophoretic diffusion coefficient	$m^2 \cdot s^{-1}$
q_r	Radiative heat flux (Rosseland approximation)	$W \cdot m^{-2}$
G	Gravitational acceleration	$m \cdot s^{-2}$
Kr	Chemical reaction rate constant	s^{-1}
U_w	Wall stretching velocity	$m \cdot s^{-1}$
τ_w	Wall shear stress	$N \cdot m^{-2}$
Q	Volumetric heat source/sink	$W \cdot m^{-3}$
$\alpha = k/(\rho c_{\mathrm{p}})$	Thermal diffusivity	$m^2 \cdot s^{-1}$
ϕ	Volume fraction of nanoparticles	—
η	Similarity variable	—
$f(\eta)$	Dimensionless stream function	—
$\theta(\eta)$	Dimensionless temperature	—
$\phi(\eta)$	Dimensionless concentration	—
Nb	Brownian motion parameter	—
Nt	Thermophoresis parameter	—
Le	Lewis number (α/D_B)	—
Pr	Prandtl number (ν/α)	—
H	Hartmann number ($B_0L\sqrt{(\sigma/\mu)}$)	—
Ec	Eckert number ($U_w^2/(c_p\Delta T)$)	—
Re	Reynolds number (U_wL/ν)	—
β_T	Thermal expansion coefficient	K^{-1}
K_B	Boltzmann constant	(J/K)
M	Magnetization vector	(A/m)
J	Electric current density	$A \cdot m^{-2}$
Ha	Hartmann number	—
Nu	Local Nusselt number	—
Sh	Local Sherwood number	—
Cf	Skin friction coefficient	—
ψ	Stream function	$m^2 \cdot s^{-1}$

REFERENCES

1. Khan A. Machine learning—a new paradigm in nanoparticle-mediated drug delivery to cancerous tissues through the human cardiovascular system enhanced by magnetic field. Scientific Reports. 2024; 14: 22615. https://doi.org/10.1038/s41598-024-72629-z
2. Riaz A, Mehmood K, Alhamzi G, Alharbi KAM. Electroosmotic flow of cobalt-ferrite nanoparticles in water and ethylene glycol through a ciliary annulus: A biomedical application. Electrophoresis. 2024; 45 (13–14):1198–1211. https://doi.org/10.1002/elps.202300137
3. Beavers GS, Joseph DD. Boundary conditions at a naturally permeable wall. Journal of Fluid Mechanics. 1967;30(1):197–207. https://doi.org/10.1017/S0022112067001375
4. Buongiorno J. Convective transport in nanofluids. Journal of Heat

Transfer. 2006; 128(3): 240–250. https://doi.org/10.1115/1.2150834
5. Hartmann J. Theory of the laminar flow of an electrically conductive liquid in a homogeneous magnetic field. Matematisk-Fysiske Meddelelser. 1937; 15(7): 1–28.
6. Mishra NK. Computer simulation of heat and mass transfer effects on nanofluid flow of blood through an inclined stenosed artery with Hall Effect. Acta Mechanica et Automatica. 2024;18(1):129–138. https://doi.org/10.2478/ama-2024-0017
7. Muhammad K, Sarfraz M. The role of Brownian diffusion and thermophoresis in optimizing energy and mass transfer for Newtonian and non-Newtonian fluids: A Keller–Box numerical study. Case Studies in Thermal Engineering. 2025; 72: 106365. https://doi.org/10.1016/j.csite.2025.106365
8. Muhammad K, Sarfraz M, Ebaid A, Elmannai H.Optimization of energy transport via electro-thermal hybrid nanofluid in parallel disks: A Keller-Box simulation. Chaos, Solitons & Fractals. 2025;198:116621. https://doi.org/10.1016/j.chaos.2025.116621
9. Nield DA. The Beavers–Joseph boundary condition and related matters. Transport in Porous Media. 2009; 78(3): 537–540. https://doi.org/10.1007/s11242-009-9344-y
10. Dolui S, Bhaumik B, De S. Combined effect of induced magnetic field and thermal radiation on ternary hybrid nanofluid flow through an inclined catheterized artery with multiple stenosis. Chemical Physics Letters. 2023; 811:140209. https://doi.org/10.1016/j.cplett.2022.140209
11. Sarfraz M. Synergistic effects of cadmium telluride and graphite nanoparticles studied with entropy analysis using the Keller–Box method. International Communications in Heat and Mass Transfer. 2025; 163: 108667. https://doi.org/10.1016/j.icheatmasstransfer.2025.108667
12. Sheikholeslami M, Ganji DD, Javed MY, Ellahi R. Effect of thermal radiation on magnetohydrodynamics nanofluid flow and heat transfer by means of two phase model. Journal of Magnetism and Magnetic Materials. 2015;374:36–43. https://doi.org/10.1016/j.jmmm.2014.08.021
13. Mnisi P, Dlamini P, Kunene TJ. Numerical Analysis of Heat Transfer in Nanofluids Flowing over a Stretching Surface Under Oscillating Magnetic Fields: Crank–Nicolson Finite Difference Method. Engineering Proceedings. 2026;132(1):5. https://doi.org/10.3390/engproc2026132005
14. Ivanov AO, Camp PJ. Magnetization relaxation dynamics in polydisperse ferrofluids. Physical Review E. 2023;107:034604. https://doi.org/10.1103/PhysRevE.107.034604
15. Fang A. Generic theory of the dynamic magnetic response of ferrofluids. arXiv preprint. 2020. https://arxiv.org/abs/2011.07277
16. Shliomis MI, Smorodin BL. Convective instability of magnetized ferrofluids.Journal of Magnetism and Magnetic Materials. 2002;252: 197–202. https://doi.org/10.1016/S0304-8853(02)00712-6
17. Sheikholeslami M, Ganji DD. Nanofluid flow and heat transfer in a rotating system in the presence of a magnetic field. Journal of Molecular Liquids. 2014;190:112–120. https://doi.org/10.1016/j.molliq.2013.11.002
18. Zhou X, Thomas BG. Measuring heat transfer during spray cooling using controlled induction-heating experiments and computational models. Applied Mathematical Modelling. 2013;37(5):3181–3192. https://doi.org/10.1016/j.apm.2012.07.039
19. Siddique I, Nadeem MM, Shakoor B, Kraiem H, Ghallab AS, Yaseen ZM, Abdullaeva B. ANN-based analysis of MHD third-grade hybrid nanofluid flow over a thin needle with fuzzy volume fraction under nonlinear radiation and heat generation. Scientific Reports. 2025; 15: 45030. https://doi.org/10.1038/s41598-025-29013-2
20. Gifty GP, Padhi SB, Mahatha BK, Mahato GK. Effects of natural convection and radiation on MHD stagnation point nanofluid flow past a stretchable surface with velocity slip and Newtonian heating. East European Journal of Physics. 2025; 3: 209–222. https://doi.org/10.26565/2312-4334-2025-3-18
21. Sheremet MA, Dinarvand S, Pop I. Effect of thermal stratification on free convection in a square porous cavity filled with a nanofluid using the Tiwari and Das nanofluid model. Physica E: Low-dimensional Systems and Nanostructures 2015; 69: 332–341. https://doi.org/10.1016/j.physe.2015.02.005

Binyam Zigta Teferi: https://orcid.org/0000-0003-4300-0812